Nitrogen isotope homogenization of dissolved ammonium with depth and 15N enrichment of ammonium during incorporation into expandable layer silicates in organic-rich marine sediment from Guaymas Basin, Gulf of California

Toshiro Yamanaka, Arisa Sakamoto, Kanon Kiyokawa, Jaeguk Jo, Yuji Onishi, Yoshihiro Kuwahara, Ji-Hoon Kim, Lucie Pastor, Andreas Teske, Daniel Lizarralde, et al.

Chemical Geology 666 (2024) 122203

Contents lists available at ScienceDirect

Chemical Geology

journal homepage: www.elsevier.com/locate/chemgeo

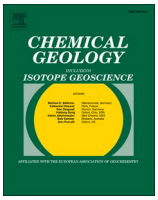

Nitrogen isotope homogenization of dissolved ammonium with depth and ^{15}N enrichment of ammonium during incorporation into expandable layer silicates in organic-rich marine sediment from Guaymas Basin, Gulf of California

Toshiro Yamanaka [a,*], Arisa Sakamoto [a], Kanon Kiyokawa [a], Jaeguk Jo [b], Yuji Onishi [c], Yoshihiro Kuwahara [d], Ji-Hoon Kim [e], Lucie C. Pastor [f], Andreas Teske [g], Daniel Lizarralde [h], Tobias W. Höfig [i], the IODP Expedition 385 Scientists

[a] School of Marine Resources and Environment, Tokyo University of Marine Science and Technology, 4-5-7 Konann, Minato-ku, Tokyo 108-8477, Japan
[b] Department of Geoenvironmental Sciences, Kongju National University, Gongju 32588, South Korea
[c] Research Institute for Humanity and Nature, 457-4 Motoyama, Kamigamo, Kita-ku, Kyoto 603-8047, Japan
[d] Division of Environmental Changes, Faculty of Social and Cultural Studies, Kyushu University, 744 Motooka, Fukuoka 819-0395, Japan
[e] Petroleum and Marine Research Division, Korea Institute of Geoscience & Mineral Resources, Daejeon 305-350, Republic of Korea
[f] IFREMER, Centre de Brest, 29280 Plouzané, France
[g] Department of Marine Sciences, University of North Carolina at Chapel Hill, Chapel Hill, NC 27599, USA
[h] Department of Geology and Geophysics, Woods Hole Oceanographic Institution, Woods Hole, MA 02543, USA
[i] International Ocean Discovery Program, Texas A&M University, College Station, TX 77845, USA

ARTICLE INFO

Editor: Vasileios Mavromatis

Keywords:
Nitrogen isotopes
Early diagenesis
Ammonium
IODP
Expedition 385
JOIDES Resolution

ABSTRACT

Sedimentary nitrogen isotopic ratios are used as a proxy for ancient biogeochemical cycles on Earth's surface. It is generally accepted that sediment hole tops record primary signatures because organic nitrogen (ON) is predominant in this part of the hole. In contrast to such early to middle diagenetic stages, it is well known that heavier nitrogen isotope ^{15}N tends to enrich in sedimentary rocks during later diagenetic and metamorphic stages. However, there are some critical gaps in our understanding of nitrogen isotopic alteration associated with abiotic processes during early-middle diagenesis. In this study, we examined the isotope ratios of ammonium nitrogen in interstitial water (IW) and total nitrogen (TN), including exchangeable ammonium and mineral nitrogen, in the solid-phase of organic-rich-sediment recovered by International Ocean Discovery Program (IODP) Expedition 385 cores drilled in the Guaymas Basin, Gulf of California, that contained ammonium-rich IW. The isotopic ratios ($\delta^{15}N$ value) of TN are the most variable with depth compared to any other type of nitrogen. This variation can be interpreted as reflecting changes in the water mass environment in the basin caused by glacial–interglacial climate changes, modifying the $\delta^{15}N$ values of the marine primary producers. Thus, the $\delta^{15}N$ value of TN is a proxy for environmental change in the basin, while each component of TN shows different trends. The $\delta^{15}N$ values of IW and exchangeable ammonium did not exhibit significant changes with depth, but the latter values are about 3 ‰ enriched in ^{15}N. This may be due to advective transport of solute into adjacent layers followed by the formation of an isotopic equilibrium between IW and exchangeable ammonium in the case of fast sediment accumulation rate. The $\delta^{15}N$ value of exchangeable ammonium is the highest among the other types of nitrogen with one exception, where the $\delta^{15}N$ value of TN is the highest. The calculated $\delta^{15}N$ values of ON based on mass balance are almost the same as those of associated TN in the shallow sediment layers (< 150 m below seafloor), but the difference in the $\delta^{15}N$ values of TN and ON are significant in the deeper layers, where proportions of ON contents are <50%. In particular, in the layer where the $\delta^{15}N$ value of TN is the highest, that of ON shows an even higher value and the difference reaches 3.5 ‰. The $\delta^{15}N$ values of mineral nitrogen are similar to that of IW ammonium except the surface layers. Under such conditions, when $\delta^{15}N$ value of TN is intermediate between those of mineral nitrogen and exchangeable ammonium, calculated $\delta^{15}N$ value of ON is close to that of TN. On the other hand, if $\delta^{15}N$ value of TN is out of the range between mineral nitrogen and exchangeable

* Corresponding author.
E-mail address: t.yamanaka@kaiyodai.ac.jp (T. Yamanaka).

https://doi.org/10.1016/j.chemgeo.2024.122203
Received 30 January 2024; Received in revised form 29 May 2024; Accepted 31 May 2024
Available online 1 June 2024

ammonium, it causes further difference in $\delta^{15}N$ value of ON. It means that the fluctuation of $\delta^{15}N$ values of TN is reduced relative to those of ON through depth. It has been considered that $\delta^{15}N$ value of TN in sediment is similar to that of ON, and changes in the $\delta^{15}N$ value of TN due to diagenesis are limited, but in such environment ON fluctuations over depth may be slightly underestimated.

1. Introduction

Nitrogen is an essential element for life and makes up most of the atmosphere as molecular nitrogen (dinitrogen N_2), thus, existing in huge amounts on the Earth's surface. Nitrogen has two isotopes: ^{14}N and ^{15}N. Their ratio in the atmospheric dinitrogen has been used as an international standard for conventional δ notation ($\delta^{15}N$). Because of the huge reservoir of atmospheric dinitrogen the nitrogen isotope ratio has not changed significantly over geological time (Sano et al., 1998). Through biological processes, nitrogen continuously cycles in the atmosphere–biosphere–hydrosphere system and surface sediment at various redox states, i.e., from the most oxidized state nitrate (NO_3^-) to the most reduced state ammonium (NH_4^+). Those biologically mediated processes, called nitrogen biogeochemical cycle, have been traced using nitrogen isotope ratios and, consequently, produced a lot of literature.

Sedimentary rocks contain a considerable amount of fixed nitrogen (Holloway and Dahlgren, 2002). Such N is primarily derived from the burial of organic matter in marine and freshwater sediments, where it is incorporated into unconsolidated and consolidated rock as organic N or as ammonium in silicate minerals because mineral cations are replaced with ammonium ions, or ammonium gets incorporated into crystal structures. These ammonium-bearing rocks become exposed on the Earth's surface through the rock cycle, and, as they are weathered and eroded, and eventually they release the fixed ammonium (i.e., native fixed ammonium) into the environment (Nieder et al., 2011, Morford et al., 2011). Release of ammonium from minerals is used by plants as a nutrient and benefits human society as fertilizer for increasing food production (Steffens and Sparks, 1999,Morford et al., 2011). Conversely, the cycling of nitrogen between the Earth's interior and the surface is associated with plate subduction and degassing via volcanism (e.g., Mysen, 2019). Such non-biologically mediated cycle, including the rock cycle, is called geochemical cycle.

However, our understanding of ammonium (or ammonia) associated with mineral–fluid interactions during early diagenesis, a part of the geochemical cycle, is limited. Although isotopic alteration of $\delta^{15}N$ signal in the sinking particles and surface sediment associated with biological processes have been studied well (e.g., Robinson et al., 2012), the behavior of nitrogen isotopes in anoxic deeper sediments where abiogenic processes (e.g., interaction of ammonium between solid and fluid phases) prevail in addition to chemoautotrophic microbial activity is not well documented (e.g., Freudenthal et al., 2001). Nitrogen initially bound to various organic materials is transferred to silicate minerals during burial and metamorphism, typically as NH_4^+ substituting for K^+ in sheet silicates (clays and micas) and feldspars because of their similar ionic radii (Honma and Itihara, 1981). A schematic model of the ammonium incorporation into expandable layer silicates and fixation processes during the early diagenetic stage is shown in Fig. 1. Organic nitrogen (ON) is transformed principally by bacterial activity into inorganic nitrogen species during mineralization in sediment, yielding ammonium (NH_4^+) as the final product (Schidlowski et al., 1983). Altabet et al. (1999) and Pride et al. (1999) found no evidence of diagenetic alteration in the $\delta^{15}N$ values of preserved organic matter in the California margin basins (USA) and in the Gulf of California (Mexico). Prokopenko et al. (2006) also reported that the isotopic ratio of ammonium–nitrogen dissolved in the interstitial water (IW) squeezed from deep marine sediments (~ 250 m below seafloor) was similar to the associated organic matter within the range of 0.4 ‰. Thus, isotopic fractionation was concluded to be negligible during early diagenesis. However, these studies measured only total nitrogen (TN) in sediments or dissolved ammonium in interstitial water together with TN. Therefore, there is a lack of systematic analysis of all nitrogen species in marine sediment. These species encompass the components of TN – organic nitrogen, mineral nitrogen (MN), and exchangeable ammonium in interlayer space of sheet silicates (clay minerals) – as well as IW ammonium and dissolved organic nitrogen as those nitrogen species contained in fluids. Here, we report results obtained from six of the eight sites drilled in the Guaymas Basin in the Gulf of California during International Ocean Discovery Program (IODP) Expedition 385 (Fig. 2). The basin marks a young spreading center to the north of the northern

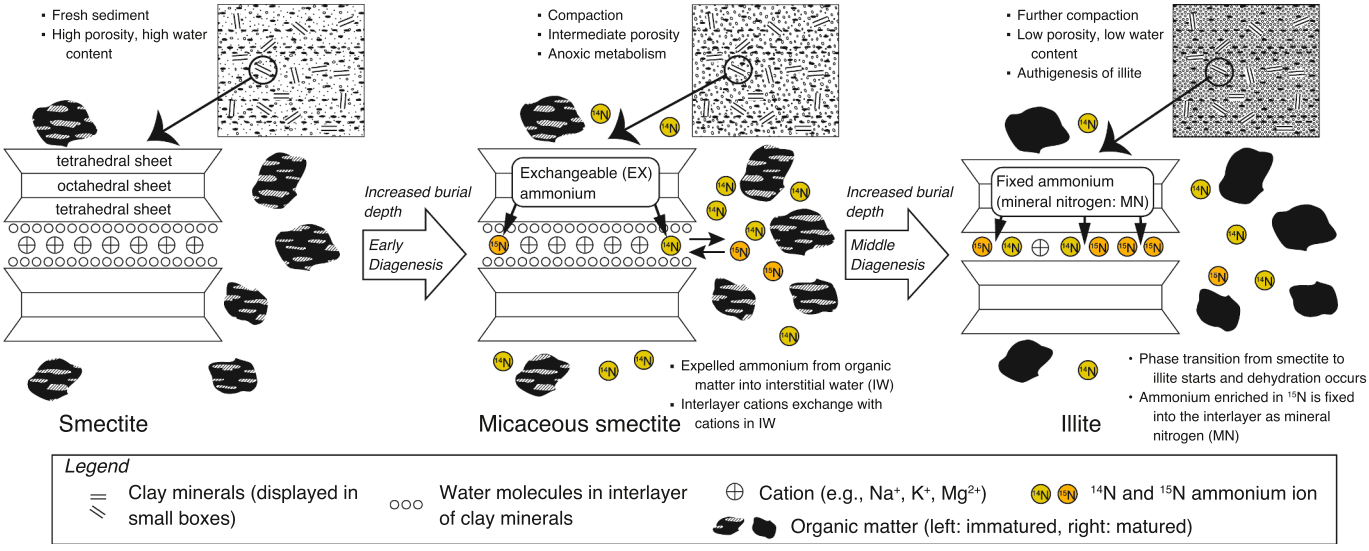

Fig. 1. Expected ammonium behavior associated with mineral–fluid interactions at early-middle diagenetic stage. In an ammonium-rich environment, cations adsorbed in the interlayers of smectite (expandable layer silicate) exchange with ammonium in ambient fluid (interstitial water: IW), and the cations are then fixed in the interlayer as mineral nitrogen (MN) with increasing burial depth.

tip of the East Pacific Rise spreading ridge that is filled with organic-rich sediment composed of mainly diatom ooze and characterized by high heat flow as well as on- and off-axis magmatism in the form of sill intrusions into sediments (Teske et al., 2021a). Jo et al. (2018) suggested that a high-ammonium environment associated with hydrothermal activity is expected to enhance the formation of ammonium-bearing clay minerals, and then MN possibly preserves the $\delta^{15}N$ value of the ambient IW ammonium. The IW squeezed from the recovered cores during the expedition contained significantly high concentrations of ammonium (~38 mM). Thus, the cores provided an opportunity to study all the types of nitrogen mentioned above except for dissolved organic nitrogen. In this study, dissolved organic nitrogen could not be measured due to a small amount of samples. The main purpose of this study is to understand the distribution of each nitrogen type in deep marine sediments and the nitrogen isotope fractionation among them. This study provides some clues to understand the behavior of individual nitrogen isotopes in ammonium during water-rock interaction and fate of ammonium associated with diagenesis.

2. Materials and Methods

2.1. Sampling methods and lithology of sediment cores

IODP Expedition 385 drilled eight sites in the Guaymas Basin, Gulf of California (Fig. 2). Each site was drilled in multiple holes (each hole at a site is maximum ~50 m apart from each other) using the advanced piston corer (APC), half-length APC (HLAPC), extended core barrel (XCB), and rotary core barrel (RCB) systems through drill pipes lowered from the derrick of R/*V JOIDES Resolution* to the subseafloor as described by Teske et al. (2021b). The sediment samples and the physical property data used in this study were obtained from the first hole (Hole A) or fourth hole (Hole D) drilled at each site (Table 1).

The sediments recovered during the expedition from each site are mainly composed of diatom ooze and clay-rich diatom ooze. Downhole changes in lithology of all the cores were not significant enough to require a division of the site into more than one lithostratigraphic unit (Unit I), while the presence of minor yet significant downhole lithologic changes and/or changes in sediment induration and physical properties prompted the division of Unit I into four subunits (IA–ID) (Teske et al., 2021a). Lithostratigraphic columns of each site are shown in Fig. S1. These differences arise mainly from different degrees and types of diagenetic processes and overprinting that have resulted in the formation of authigenic minerals (e.g., micrite in Subunit IB) and/or the selective dissolution of sedimentary particles (e.g., dissolution of diatoms during opal-A to opal-CT phase transformation in Subunits IC and ID) except for Sites U1549 and U1552, where no major diagenetic changes were observed. In addition to those sediments, thin (< 1 m thick) and thick (~80 m) igneous rock layers (sills) were identified in the cores obtained from Sites U1545 and U1546, respectively, but all samples provided for this study were recovered from above the intersected sills as shown in Fig. S1. Only the sediments recovered at Site U1551 are rich in terrigenous clastic particles, which are composed of two parts: diatom ooze and clay with significant amount of silt- to sand-sized siliciclastic particles at upper interval (<90 meters below seafloor, mbsf) and predominantly terrigenous unconsolidated sandy particles at lower interval. A comprehensive report detailing the characteristics of each site is provided by Teske et al. (2021a).

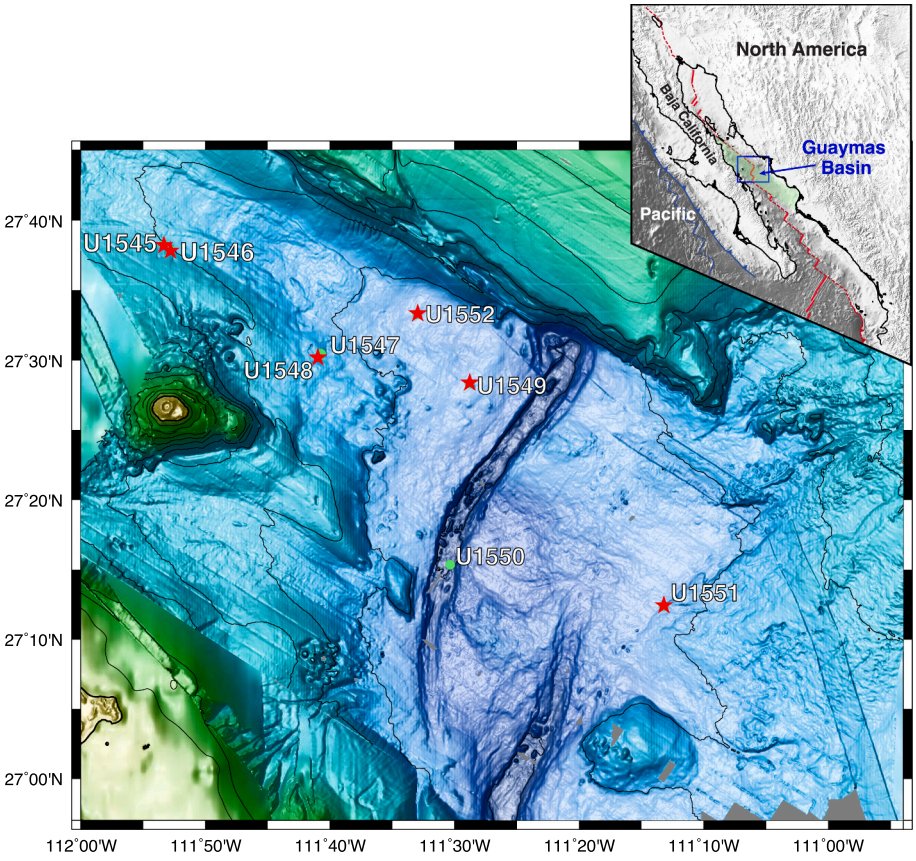

Fig. 2. Bathymetry of the Guaymas Basin with Baja California in the southwest and the Sonora margin in the northeast, showing International Ocean Discovery Program (IODP) Expedition 385 sites (U1545 – U1552) drilled in the area (modified from Teske et al., 2021a). The six sites analyzed in this study are indicated by red stars. (For interpretation of the references to color in this figure legend, the reader is referred to the web version of this article.)

Table 1
Core sample information for this study.

Site	Hole	Latitude (N)	Longitude (W)	Water depth (m below sea level)	Total penetration (m)	Core recovered (m)	Recovery (%)
U1545	A	27°38.23′	111°53.34′	1593.5	503.3	389.0	77.3
U1546	D	27°37.89′	111°52.78′	1585.9	300.1	314.7	104.9
U1548	D	27°30.53′	111°41.39′	1729.3	110.0	120.5	109.6
U1549	A	27°28.33′	111°28.78′	1840.1	168.0	166.9	99.3
U1551	A	27°12.39′	111°13.19′	1844.1	120.3	122.1	101.5
U1552	A	27°33.29′	111°32.97′	1841.6	107.5	73.9	68.7

2.2. Onboard processing of sediment cores

IW extraction was conducted aboard the R/*V JOIDES Resolution* using a titanium squeezer (Manheim and Sayles, 1974) according to the following procedure described by Teske et al. (2021b). Squeezed IW was collected in a precleaned (10% HCl) high-density polyethylene (HDPE) syringe attached to the squeezing assembly and subsequently filtered through a polyethersulfone membrane disposable filter (pore size = 0.2 μm). The residual sediment in the squeezer (so-called squeezed cake) was divided into several parts and immediately stored in the freezer (*c.* –20 °C).

The IW samples were analyzed on board following the protocols outlined by Gieskes et al. (1991), Murray et al. (2000), and the IODP user manuals for shipboard instrumentation (http://iodp.tamu.edu/labs/documentation), which were updated during Expedition 385. According to the methods in these protocols, ammonium concentrations in the IW samples were measured using the indophenol method and colorimetric analysis. For more details on IW inorganic geochemistry see the IODP Expedition 385 methods (Teske et al., 2021b).

For onshore analyses, the IW samples were quickly frozen in a deep

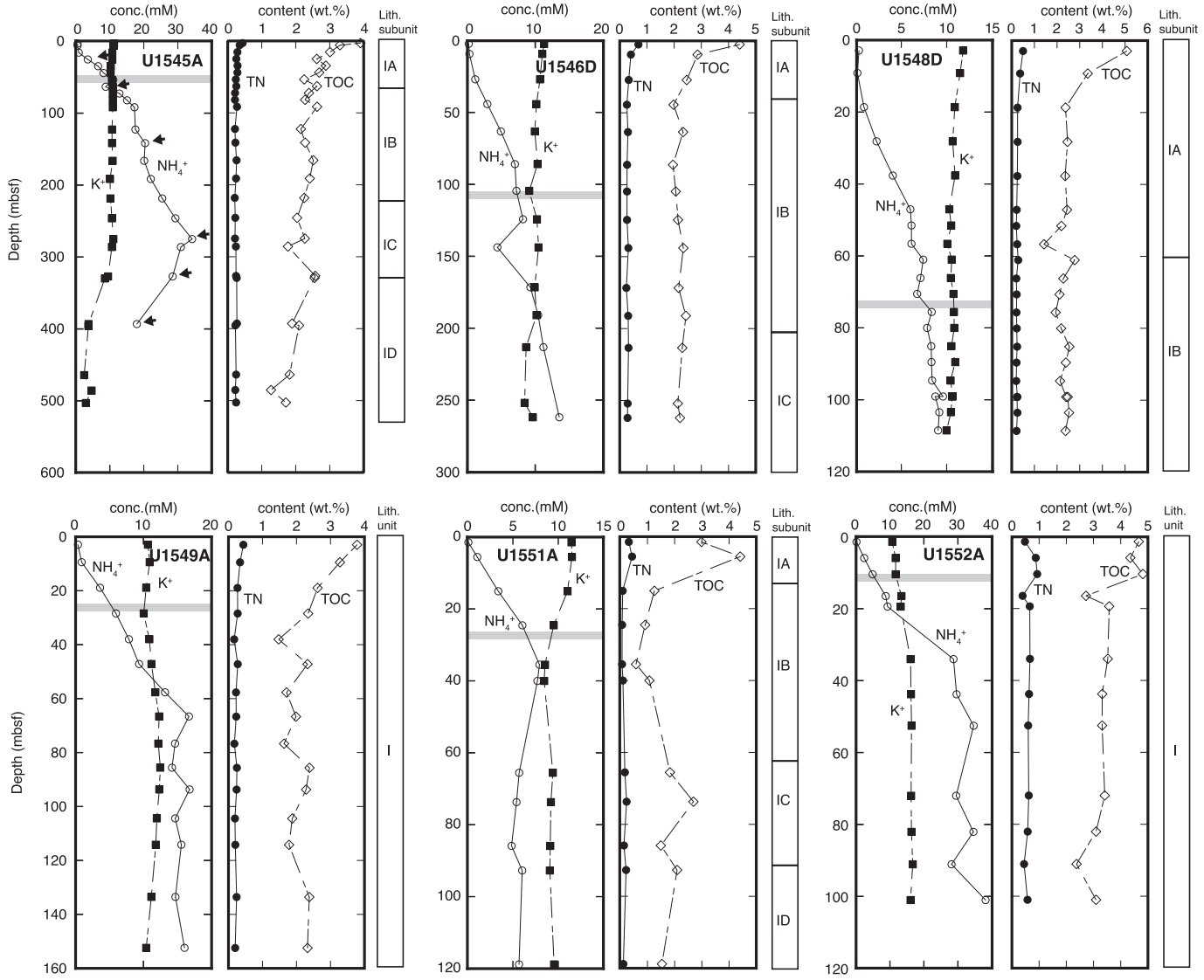

Fig. 3. Downhole profiles of the concentrations (mM) in ammonium (open circle) and potassium (filled square) dissolved in interstitial water samples and TOC (filled circle) and TN (open diamond) contents (wt%) in sediment samples from the six holes studied, shown with lithostratigraphic subunits. Small arrows in the ammonium profile of Hole U1545A indicate the six selected samples provided for further analyses. Gray horizontal lines indicate sulfate–methane transition zones (SMTZ).

freezer at −80 °C on board and stored in a freezer at −30 °C until just before analyses took place.

2.3. Mineralogical and geochemical analyses of sediment samples

TN and total organic carbon (TOC) contents as well as their nitrogen and carbon isotope ratios ($\delta^{15}N_{TN}$ and $\delta^{13}C_{TOC}$) in the bulk sediment samples (squeezed cakes), respectively, were measured using an elemental analyzer coupled with an isotope ratio mass spectrometer (EA/irMS), GV Instruments IsoPrime EA at the Tokyo University of Marine Science and Technology (TUMSAT). For TOC analysis, sediment samples were weighed and placed into silver capsules, then spiked 6 N HCl for digestion of inorganic carbon minerals (carbonates). The flash combustion method, i.e., short-time burning in an elemental analyzer, has turned out to yield insufficient amounts of nitrogen in highly consolidated silicate minerals, especially in low nitrogen-content samples (Bräuer and Hahne, 2005). However, the samples provided for this study were unconsolidated and contained sufficient amount of nitrogen (≥ 600 ppm). Therefore, it is expected that at least 90% yielding of nitrogen and analytical error for nitrogen isotopic ratio is lower than ±1 ‰.

In addition to the bulk analyses, the clay fraction (≤2 μm) was separated from the six selected sediment samples (squeezed cakes) obtained from the Hole U1545A core material through gravity sedimentation, i.e., the recovered suspension load up to a depth of 10 cm from suspending bulk samples in distilled water after 8 h according to Stokes' law. The positions of six samples indicated in Fig. 3 show that at least one sample was taken from each lithostratigraphic unit. The recovered clay fractions underwent a rigorous treatment process, including three successive exposures to a warm 30% hydrogen peroxide solution and finally to an alkaline potassium hypobromite (KOBr–KCl) solution, to eliminate organic matter from the fractions (Black et al., 1965; Silva, 1964; Silva and Bremner, 1966). Black and his colleagues established a method for separately purifying inorganic nitrogen contained in soil and sediment in the 1960s (Black et al., 1965), and no new methods have been developed since then. The KOBr–KCl solution is a suitable reagent for eliminating ON compounds without affecting MN in clay minerals (Black et al., 1965). The residual nitrogen in the sample after the treatment is defined as MN (Liang et al., 1999), which is expected to be mostly fixed ammonium in the interlayers of 2:1 type clay minerals. Non-clay fraction (>2 μm) was also eliminated ON in the same manner. The nitrogen content of MN and its isotopic ratio were determined using an elemental analyzer coupled with isotope-ratio mass spectrometer (EA/irMS).

Minerals in the clay fractions were identified by X-ray diffraction (XRD), using a Rigaku Ultima IV at TUMSAT. XRD measurements were performed at 40 kV and 40 mA using Ni-filtered Cu-Kα (λ = 1.5418 Å) radiation. Step-scan XRD analysis was performed on the bulk powder (random) samples (2°–70° 2θ, 0.02° 2θ step width, 10 s/step) and clay fraction samples (2°–40° 2θ, 0.02° 2θ step width, 10 s/step) oriented on glass slides after Mg^{2+} and ethylene glycol treatment. Measurement of crystallinity of illite and relative amount of clay minerals were made by using decomposition procedure of X-ray diffraction (XRD) patterns described by Kuwahara et al. (2001).

Fourier-transform infrared spectroscopy (FT-IR) analysis was performed on the bulk and clay fraction samples. The spectra of the powder samples were recorded in the region ranging from 4000 to 600 cm^{-1} with a resolution of 4 cm^{-1}, and averaged over 32 scans using JASCO FT/IR-6100 at TUMSAT. Subsequently, the spectral data were interpreted using Spectragryph ver.1.2.16, an optical spectroscopy software. Baseline correction was applied equally to all samples.

EX ammonium in the squeezed cakes was extracted using a 2-M KCl solution on a shaker overnight. The concentration of the extracted ammonium–nitrogen was measured using the steam distillation technique originally described by Bremner and Edwards (1965) using a gas-tight container, followed by volumetric titration using a methyl red and bromocresol green mixture as a color indicator. The method for measuring the nitrogen isotopic ratio is described below.

According to the above descriptions, the terms used in this study are defined as follows:

IW ammonium: dissolved ammonium in IW squeezed from the core sediment immediately after recovered on deck. Its nitrogen isotopic ratio is expressed in $\delta^{15}N_{IW\text{-}amm}$.

EX ammonium: exchangeable ammonium extracted from the sediment after squeezing IW using KCl solution by shaking overnight. Its nitrogen isotopic ratio is expressed as $\delta^{15}N_{EX\text{-}amm}$.

MN: mineral nitrogen, which is the residual nitrogen in the sediment after the KOBr–KCl treatment. Its nitrogen isotopic ratio as expressed as $\delta^{15}N_{MN}$.

ON: organic nitrogen, which is a solid in the squeezed cake and can be removed by KOBr–KCl treatment. Its nitrogen isotopic ratio as expressed as $\delta^{15}N_{ON}$.

The overall analytical reproducibility during the aforementioned processes is estimated to be ±0.5% for quantitative analyses and better than ±0.3 ‰ for isotope ratio analyses. In this study, all isotopic values are expressed in the common $\delta^{15}N$ and $\delta^{13}C$ notations, per mil deviation relative to international standards, atmospheric dinitrogen and Vienna-Pee Dee Belemnite, respectively.

2.4. Chemical and isotopic analyses of fluid samples

Aliquots of ammonium-rich fluid (IW) samples (≥1 mM and ≥ 4 ml) were subject to shore-based nitrogen isotopic ratio analysis for ammonium. IW ammonium was recovered by the steam distillation technique using a gas-tight container as mentioned above and finally converted into ammonium sulfate [$(NH_4)_2SO_4$] (Mizota et al., 2007). As a common knowledge of stable isotope geochemistry of light elements, evaporation followed by condensation accompanies a distinctive isotopic fractionation. The process is well known for penguin colony in Antarctica (Mizutani et al., 1985). During the microbial-mediated transformation of uric acid in fecal droppings on the ground, residual fractions tend to be enriched in ^{15}N, whereas emitted NH_3 tends to be enriched in ^{14}N. Based on the evidence, we were sufficiently careful to determine the precious isotopic ratios of ammonium. Ammonium in the distillates was trapped by presence of excess H_2SO_4 where no further modification of the isotopic signature of the intrinsic ammonium in sample materials occurs. Higher than 98% recovery of ammonium was confirmed by distillation of standard solution (1 ml of 16 mM $(NH_4)_2SO_4$ solution), testing every day before run of sample distillation. The ammonium sulfate solution was concentrated by gentle evaporation on a hot plate (~75 °C). Then the solution was soaked using a small piece of glass fiber filter and dried in an oven at 60 °C. The pieces of the filter were installed in the EA/irMS to determine the nitrogen isotopic ratio ($\delta^{15}N_{IW\text{-}amm}$). Analytical reproducibility is estimated to be ±0.5% for quantitative analysis and better than ±0.3 ‰ for isotope ratio analysis.

2.5. Calculations of contents and nitrogen isotopic ratios of ON in the sediment and terminologies employed in this study

As described above, we measured four types of nitrogen, i.e., TN, MN, and EX ammonium in clay minerals and dissolved ammonium in IW. Organic compounds, such as protein (amino acids), nucleobase and porphyrin, are considered to be the major carrier of sedimentary nitrogen in solid phase (excluding IW ammonium). Here we assume that sedimentary nitrogen comprises ON, MN, and EX ammonium. Therefore, the ON content is calculated as follows:

$$[ON] = [TN] - ([MN] + [EX\ ammonium]) \ (unit: \mu g\ N/g\ dry\ sediment)$$

Following the above assumption, the $\delta^{15}N_{ON}$ value is calculated based on the basis of the mass balance equation:

$$\delta^{15}N_{TN} = a \times \delta^{15}N_{ON} + b \times \delta^{15}N_{ex-amm} + c \times \delta^{15}N_{MN}$$

where a, b, and c represent the relative abundance of each type of sedimentary nitrogen ($a + b + c = 1$). After the calculation, errors of the ON contents and $\delta^{15}N_{ON}$ values are estimated using the law of error propagation, 1% and 0.6 ‰, respectively.

In this study, diverse forms of nitrogen in both solid and fluid phases are delineated. The term "content" is employed to indicate the amount of nitrogen per unit mass of solid (e.g., MN content in a gram of dry sediment; g N/g dry sediment, in the case of TN and TOC, referring to wt %). By contrast, the term "concentration" indicates the amount of nitrogen per unit volume of fluid (e.g., ammonium concentration in IW; mol/L or M). Subsequently, the IW ammonium content is calculated as follows:

$$\text{IW volume } (cm^3) \text{ in } 1 - cm^3 \text{ bulk wet sediment} = (\text{wet density–dry density})/1.024 = V$$

$$\text{IW ammonium content } (\mu g\ N/g \text{ dry sediment}) = \text{concentration of IW ammonium } (\mu mol/L) \times V - cm^3 \times \text{mass number of N } (=14.01)/\text{dry density } (\text{g dry weight}/\text{bulk } 1\ cm^3)$$

where wet and dry densities of the sediment are obtained from the IODP shipboard data available online (Laboratory Information Management System (LIMS) Online Reports; https://web.iodp.tamu.edu/LORE/). The factor 1.024 refers to the density of seawater in g/cm^3.

3. Analytical results

3.1. Ammonium concentrations dissolved in IW and lithology of the sediment cores

Table 2 displays both onboard and onshore analytical data of the six sites studied. This table also shows the associated lithostratigraphic units as defined by the shipboard lithological and mineralogical studies reported by Teske et al. (2021a).

Although the depths that reached maximum concentrations of IW ammonium in each hole are different, ranging from 40 to 300 mbsf, these concentrations increase downhole until the middle or bottom of the Unit IC, and then decrease downhole as shown in Fig. 3. The maximum concentrations of IW ammonium reach up to 38 mM and vary from 7.9 to 38 mM among the holes.

3.2. Contents of TOC, TN, EX ammonium, and MN in the core sediments

The TOC and TN contents in the sediment samples (squeezed cake) and the IW ammonium dissolved in squeezed IW for all holes studied are shown in Table 2. The vertical profiles of those data are shown in Fig. 3. The highest values of TOC and TN in each hole (3–5 wt% and 0.3–0.7 wt %, respectively) were measured in the shallowest samples of each hole and show a rapid decrease in the concentrations to a depth of 50 m from the seafloor. Further downhole, the concentrations are virtually constant, especially with respect to TN values except for TOC in the Hole U1551A. In Table 2, the atomic TOC/TN values (C/N values) are also shown. The minimum and maximum average C/N value of each hole is 6.4 for U1552A cores and 12.7 for U1551A cores. The standard deviation (S.D.) of C/N values for each hole is <1.6 except for Hole U1551A (S.D. = 3).

In addition to TOC and TN contents, the EX ammonium extracted from the squeezed cake samples and the MN content in the clay and non-clay fractions of the selected six samples in Hole U1545A are summarized in Table 3 and plotted as vertical profiles in Fig. 4, along with the content of IW ammonium involved in a 1-g dry sediment. TN is the most abundant in this hole while the other types of nitrogen are one or two orders of magnitude lower than TN. Although the contents of TN show very small variation except for the shallow layer (Fig. 3), variations of the other types of nitrogen are much more pronounced (Fig. 5). The IW and EX ammonium contents increase downhole to a depth of 100 mbsf, below which they remain almost constant to the depth of 300 mbsf. Below this depth, the IW ammonium content significantly decreases, whereas the EX ammonium content dose not vary significantly. Although the contents of MN in clay and non-clay fractions are low compared with the other types of nitrogen, they show elevated values, correlating with the decrease of IW ammonium, in the bottom layers of Hole U1545A. Especially in the deepest layer the sum of both MN contents accounts for 54% of TN.

3.3. $\delta^{13}C$ and $\delta^{15}N$ values of TOC, TN, IW ammonium in the sediments

The $\delta^{13}C$ and $\delta^{15}N$ values of TOC, TN, and IW ammonium are summarized in Table 2. Their downhole profiles are shown in Fig. 5. The $\delta^{13}C_{TOC}$ and $\delta^{15}N_{IW\text{-}amm}$ values in each core vary within very narrow ranges (S.D. < 1 ‰) and those averages are −21.3 to −22.0 ‰ and + 7.1 to +10.5 ‰, respectively, except for $\delta^{13}C_{TOC}$ in Holes U1551A and U1552A (S.D. = 1.3 and 1.2 ‰, respectively) and $\delta^{15}N_{IW\text{-}amm}$ in Hole U1552A (S.D. = 1.3 ‰) as shown in Table 2. On the other hand, $\delta^{15}N_{TN}$ values vary widely from +7.3 to +16.5 ‰ with an average range of +10.0 to +13.1 ‰.

3.4. $\delta^{15}N$ values of EX ammonium, MN, and ON in the Hole U1545A sediments

The vertical profiles of $\delta^{15}N$ values for EX ammonium, MN, and ON in the six selected samples of Hole U1545A are summarized in Table 3 and plotted as vertical profiles in Fig. 4. The $\delta^{15}N$ values of TN and IW ammonium in the same layers are also plotted. The average $\delta^{15}N_{MN}$ values in clay and non-clay fractions are lower than those of the other types of nitrogen (+9.2 and + 8.6 ‰, respectively; Table 3). The profiles of these $\delta^{15}N$ values are similar to each other and increase downhole until 300 mbsf. On the other hand, the average $\delta^{15}N_{EX\text{-}amm}$ value is +13.5 ‰, being the highest value among the six types of nitrogen (Table 3). These $\delta^{15}N$ values do not vary with depth; thus, the S.D. is only 0.3 ‰.

The calculated $\delta^{15}N_{ON}$ values at each layer are very similar to those of TN until the depth of 150 mbsf, because ON is the most abundant nitrogen species in each sediment sample. However, the $\delta^{15}N_{ON}$ values are distinguishable from those of TN in the deeper layers, where ON contents are <50%.

Table 2
Quantitative and isotopic data of TN, TOC, and IW ammonium obtained from the six holes studied.

Site	Hole	Sample ID	Depth (mbsf)	Lithostratigraphic (Sub)unit	TN		IW NH_4^+		TOC		TOC/TN
					content (wt%)	$\delta^{15}N$ (‰)	conc. (mM)	$\delta^{15}N$ (‰)	content (wt%)	$\delta^{13}C$ (‰)	atomic ratio
U1545	A	1H_2_IW_145–150	2.97	IA	0.435	+10.7	0.56	+9.1	3.905	−20.4	10.48
		2H_1_IW_145–150	5.95		0.350	+10.9	0.53	+10.7	3.300	−20.6	11.01
		3H_1_IW_145–150	15.45		0.286	+13.4	0.86	+10.6	3.009	−21.0	12.27
		4H_1_IW_146–151	24.96		0.253	+8.4	3.53	+10.4	2.621	−20.8	12.10
		5H_1_IW_145–150	34.45		0.289	+9.3	6.58	+10.1	2.886	−20.0	11.64
		6H_1_IW_145–150	43.95		0.286	+9.9	8.17	+10.5	2.691	−20.5	10.98
		7H_1_IW_145–150	53.45		0.239	+11.8	11.03	+10.3	2.247	−21.1	10.98
		8H_1_IW_146–151	62.96	IB	0.254	+12.2	8.79	+11.6	2.622	−21.5	12.04
		9H_1_IW_136–141	72.36		0.214	+12.7	12.83	+10.8	2.389	−21.0	13.01
		10H_1_IW_136–141	81.86		0.212	+13.2	15.09	+10.8	2.278	−21.5	12.54
		11H_2_IW_134–139	91.59		0.272	+10.6	17.25	+10.2	2.626	−20.9	11.27
		14H_3_IW_123–128	122.39		0.212	+11.1	17.55	+10.4	2.152	−21.7	11.83
		17F_2_IW_141–146	141.41		0.224	+11.0	20.39	+9.5	2.277	−21.2	11.84
		23F_2_IW_135–140	165.92		0.261	+11.7	20.11	+9.6	2.518	−21.8	11.25
		29F_3_IW_121–126	191.28		0.244	+12.8	22.07	+10.4	2.413	−22.2	11.52
		34F_1_IW_110–115	218.20		0.205	+14.1	25.45	+10.9	2.251	−22.5	12.82
		41F_1_IW_145–150	245.85	IC	0.220	+15.3	29.32	+9.6	2.040	−21.7	10.80
		47F_2_IW_107–112	274.71		0.210	+16.5	34.21	+10.3	2.268	−22.4	12.58
		51X_1_IW_122–127	285.82		0.241	+10.7	30.94	+10.0	1.772	−22.2	8.58
		55X_3_IW_129–144	326.73		0.242	+13.4	28.47	+9.8	2.572	−22.7	12.38
		55X_5_IW_125–145	329.62		0.262	+12.9	–	+10.0	2.554	−21.7	11.38
		62X_1_IW_135–150	392.85	ID	0.270	+9.9	17.96	+10.2	1.891	−22.2	8.18
		65X_5_IW_115–130	395.50		0.223	+10.9	–	+11.0	2.097	−21.3	10.95
		69X_3_IW_136–151	463.97		0.248	+9.7	–	+10.5	1.819	−21.3	8.55
		72X_1_IW_124–139	485.34		0.223	+10.0	–	+10.3	1.274	−21.1	6.67
		74X_3_IW_125–145	502.76		0.247	+10.1	–	+10.1	1.711	−22.3	8.07
			Av.		0.25	+11.7		+10.3	2.39	−21.5	11.0
			S.D.		0.05	1.9		0.5	0.53	0.7	1.6
			p value*		c	n.a.	n.a.	a	b	a	a
U1546	D	1H_2_IW_100–120	2.51	IA	0.685	+11.3	0.26	+10.6	4.409	−20.3	7.51
		2H_4_IW_100–120	9.51		0.410	+12.0	0.37	+11.1	2.859	−21.7	8.08
		4H_3_IW_120–140	27.16		0.330	+8.6	1.22	+10.4	2.463	−21.2	8.74
		6H_2_IW_90–110	44.40	IB	0.260	+11.0	3.00	+11.3	1.975	−21.4	8.74
		8H_2_IW_90–110	63.41		0.300	+12.4	5.00	+11.4	2.330	−20.9	9.15
		10H_5_IW_30–50	86.12		0.270	+9.0	7.05	+10.6	1.956	−21.7	8.47
		14H_2_IW_120–140	104.70		0.265	+10.7	7.29	+10.1	2.061	−21.1	9.08
		16H_3_IW_45–65	124.46		0.265	+11.9	8.24	+9.7	2.141	−22.1	9.42
		18H_3_IW_102–122	144.04		0.315	+10.0	4.48	+9.8	2.338	−21.5	8.65
		21H_3_IW_30–50	171.77		0.240	+14.2	9.33	+9.9	2.166	−21.9	10.50
		23H_3_IW_70–90	191.12		0.310	+10.3	10.47	–	2.431	−21.8	9.10
		27H_3_IW_35–55	213.41	IC	0.320	+13.1	11.24	–	2.296	−22.8	8.40
		35F_2_IW_110–130	252.11		0.290	+13.0	–	–	2.133	−22.5	8.58
		37F_3_IW_40–60	262.09		0.285	+12.1	13.58	–	2.216	−21.9	9.06
			Av.		0.32	+11.4		+10.5	2.41	−21.6	8.8
			S.D.		0.11	1.6		0.6	0.62	0.6	0.7
			p value*		b	n.a.	n.a.	a	b	a	b
U1548	D	1H_2_IW_141–151	2.92	IA	0.493	+10.4	0.31	–	5.075	−22.3	9.48
		2H_2_IW_136–146	9.16		0.371	+11.8	0.14	–	3.355	−22.2	10.56
		3H_2_IW_135–145	18.65		0.257	+8.8	0.87	–	2.371	−20.5	10.78
		4H_2_IW_135–145	28.16		0.260	+7.9	2.26	–	2.457	−20.5	11.01
		5H_2_IW_135–145	37.66		0.246	+10.2	4.05	+8.2	2.359	−20.8	11.17
		6H_2_IW_126–136	47.06		0.218	+11.2	5.99	+9.3	2.441	−21.0	13.08
		6H_5_IW_135–145	51.56		0.198	+11.7	6.11	+8.9	2.189	−21.6	12.88
		7H_2_IW_135–145	56.65		0.241	+10.4	6.10	+9.7	1.425	−21.0	12.55
		7H_5_IW_141–151	61.03		0.285	+12.1	7.41	+10.5	2.775	−20.9	11.35
		8H_2_IW_135–145	66.15	IB	0.203	+12.3	7.11	+10.0	2.277	−21.1	13.07
		8H_5_IW_135–145	70.57		0.214	+9.8	6.74	+10.9	2.106	−21.9	11.46
		9H_2_IW_135–145	75.61		0.209	+7.3	8.33	+10.1	1.940	−21.5	10.84
		9H_5_IW_135–145	80.03		0.222	+9.1	7.85	+9.2	2.179	−21.5	11.46
		10H_2_IW_136–146	85.12		0.234	+9.1	8.29	+9.6	2.542	−21.3	12.67
		10H_5_IW_135–145	89.54		0.209	+10.0	8.32	+9.4	2.385	−20.8	13.28
		11H_2_IW_135–145	94.66		0.199	+9.4	8.38	+9.4	2.131	−21.5	12.50
		12H_2_IW_132–142	99.08		0.246	+8.9	9.59	+9.8	2.403	−21.4	11.38
		11H_5_IW_136–146	99.09		0.229	+11.0	8.74	+9.1	2.474	−21.5	12.59
		12H_5_IW_131–141	103.48		0.252	+9.2	9.18	+12.0	2.526	−21.6	11.71
		13F_2_IW_130–140	108.56		0.212	+9.7	9.04	+10.2	2.374	−21.5	13.07
			Av.		0.25	+10.0		+9.8	2.49	−21.3	11.8
			S.D.		0.07	1.4		0.9	0.71	0.5	1.1
			p value*		cd	n.a.	n.a.	a	b	a	a

(*continued on next page*)

Table 2 (*continued*)

Site	Hole	Sample ID	Depth (mbsf)	Lithostratigraphic (Sub)unit	TN		IW NH_4^+		TOC		TOC/TN
					content (wt%)	$\delta^{15}N$ (‰)	conc. (mM)	$\delta^{15}N$ (‰)	content (wt%)	$\delta^{13}C$ (‰)	atomic ratio
U1549	A	1H_2_IW_145–150	2.95	I	0.436	+10.9	0.37	–	3.782	−21.0	10.13
		2H_2_IW_145–150	9.45		0.340	+11.0	0.92	–	3.279	−20.9	11.25
		3H_2_IW_145–150	18.96		0.267	+12.4	3.61	+10.4	2.621	−22.0	11.44
		4H_2_IW_145–150	28.45		0.269	+10.7	5.96	+10.6	2.341	−21.5	10.16
		5H_2_IW_150–155	38.01		0.168	+11.2	7.85	+9.7	1.476	−22.0	10.24
		6H_2_IW_137–141	47.24		0.273	+11.4	9.36	+10.6	2.325	−21.2	9.95
		7H_3_IW_145–150	57.71		0.223	+9.3	13.17	+8.2	1.705	−21.2	8.93
		8H_3_IW_139–144	66.65		0.226	+13.2	16.70	+9.9	1.986	−21.5	10.24
		9H_3_IW_146–151	76.73		0.172	+13.7	14.66	+10.0	1.637	−21.8	11.13
		10H_3_IW_144–149	85.67		0.247	+13.3	14.19	+10.4	2.385	−21.1	11.26
		11H_2_IW_145–150	93.74		0.237	+12.5	16.79	+10.2	2.285	−20.8	11.24
		12H_2_IW_145–150	104.46		0.190	+14.6	14.68	+10.6	1.877	−21.5	11.55
		13H_3_IW_138–143	114.22		0.199	+10.9	15.58	–	1.781	−21.7	10.47
		15H_3_IW_141–146	133.57		0.238	+12.1	14.70	–	2.377	−22.5	11.68
		17H_3_IW_146–151	152.45		0.194	+13.7	16.03	–	2.324	−23.2	13.95
			Av.		0.25	+12.1		+10.1	2.28	−21.6	10.6
			S.D.		0.07	1.4		0.7	0.61	0.6	0.8
			p value*		cd	n.a.	n.a.	a	b	a	a
U1551	A	1H_1_IW_145–150	1.45	IA	0.312	+10.8	0.07	–	2.982	−20.8	11.17
		2H_2_IW_146–151	5.56		0.433	+11.1	1.06	–	4.411	−20.9	5.92
		3H_2_IW_145–150	15.05	IB	0.088	+6.9	3.38	–	1.255	−23.1	16.60
		4H_2_IW_145–150	24.55		0.069	+7.9	6.04	+5.5	0.915	−22.4	15.53
		5H_3_IW_145–150	35.48		0.064	+12.6	7.91	+7.2	0.576	−25.0	10.42
		6H_2_IW_145–150	40.00		0.096	+12.1	7.70	+7.0	1.069	−23.2	13.00
		10H_3_IW_140–150	65.54	IC	0.170	+12.9	5.67	+7.9	1.824	−21.7	12.49
		11H_2_IW_140–150	73.71		0.233	+11.1	5.39	+7.0	2.691	−20.7	13.49
		12H_4_IW_140–150	85.87		0.133	+9.1	4.84	+7.5	1.491	−22.1	13.11
		13H_2_IW_141–151	92.71	ID	0.213	+8.7	6.01	+7.7	2.090	−21.2	11.43
		19F_2_IW_140–150	118.81		0.112	+7.0	5.67	+6.9	1.531	−20.8	16.01
			Av.		0.17	+10.0		+7.1	1.89	−22.0	12.7
			S.D.		0.12	2.2		0.7	1.11	1.3	3.0
			p value*		d	n.a.	n.a.	b	b	a	a
U1552	A	1H_1_IW_139–149	1.39	I	0.478	+9.9	0.18	–	4.664	−22.0	11.39
		2H_2_IW_140–150	5.90		0.875	+11.3	2.47	–	4.356	−22.3	5.81
		2H_5_IW_141–151	10.41		0.926	+12.3	4.93	–	4.817	−22.5	6.07
		3H_3_IW_140–150	16.48		0.389	+11.2	8.78	+9.4	2.721	−25.8	8.15
		3H_5_IW_136–146	19.40		0.652	+12.9	9.34	+9.8	3.577	−23.0	6.41
		5H_2_IW_99–109	33.99		0.661	+12.4	28.73	+7.5	3.525	−25.3	6.23
		6H_2_IW_128–138	43.78		0.630	+12.6	29.65	+7.6	3.321	−24.2	6.15
		7H_2_IW_92–102	52.55		0.599	+13.2	34.66	+9.8	3.318	−24.2	6.47
		9H_2_IW_123–133	72.00		0.618	+13.1	29.51	+11.6	3.411	−24.7	6.44
		10H_3_IW_120–130	82.02		0.575	+14.1	34.61	+9.0	3.092	−23.7	6.27
		11H_2_IW_116–126	91.07		0.443	+16.3	28.17	+8.8	2.374	−24.7	6.25
		12H_3_IW_105–115	101.00		0.575	+14.6	38.18	–	3.090	−24.2	6.27
			Av.		0.63	+12.8		+9.2	3.42	−23.9	6.41
			S.D.		0.16	1.6		1.3	0.77	1.2	1.62
			p value*		a	n.a.	n.a.	a	a	b	c

–; not measured.
n.a.; no analysis.
Sample IDs in bold are the selected samples provided for further analyses.
* The different letters indicate significant differences ($p < 0.05$) between the values of each hole according to the Steel-Dwass test.

3.5. Mineral compositions of the sediment samples from U1545A cores

XRD patterns of the clay fractions (≤ 2 μm) obtained from the six selected samples of the Hole U1545A are shown in supplementary Fig. S2. The assemblages of identified clay minerals in the sediment samples are shown in Table 4. The sediments are rich in clay minerals, especially smectite (≥ 32 wt%), followed by illite (≥ 26 wt%). Illite and smectite mixed layer (I/S) minerals (≤ 8 wt%), chlorite (≤ 12 wt%), and kaolinite (≤ 10 wt%) were also detected in all samples. Quartz and albite were also detected in the clay and non-clay fractions of all samples.

The clay contents in the samples increase downhole (Table 4). The proportion of smectite shows an increasing trend downhole, whereas the proportions of illite, chlorite, and kaolinite show an decreasing trend downhole. The modified Lanson index (MLI: Kuwahara et al., 2001) is also shown in Table 4. The values are very low (~0.03) throughout the hole. MLI values refer to a method for evaluating the crystallinity of illite (Kuwahara et al., 2001), i.e., low MLI indicates low crystallinity of illite. The crystallinity of illite is an indication for weathering and/or hydrolysis of parent material (generally land masses) (Kuwahara et al., 2001) or evolution of diagenetic processes (Lanson, 1997). Throughout Hole U1545A, the MLI is lower than 0.1, indicating quite low crystallinity of illite (Table 4).

3.6. FT-IR analysis

The FT-IR spectra of the bulk sediment and clay fractions (after treatment with KOBr–KCl solution) in the six selected samples from Hole U1545A are shown in supplementary Figs. S3 and S4, respectively. The absorption of ammonium in all of the samples was detected through weak vibration around 1400–1500 cm^{-1} within an ammonium-bend

Table 3
Quantitative and isotopic data of TN, ON, MN, and EX ammonium in the selected six samples from Hole U1545A.

			Solid phase												Fluid phase	
			TN		exchangeable-NH_4^+		MN (clay fraction)		MN (non-clay fraction)		MN (total)		Organic-N**		IW-NH_4^+	
Core, Section	Interval (cm)	Depth (mbsf)	conc. (μg N/g*)	$\delta^{15}N$ (‰)	conc. (μg N*/g)	$\delta^{15}N$ (‰)	conc. (μg N/g)*	$\delta^{15}N$ (‰)	conc. (μg N/g)*	$\delta^{15}N$ (‰)	conc. (μg N/g*)	$\delta^{15}N$ (‰)	conc. (μg N*/g)	$\delta^{15}N$ (‰)	conc. (μg N***/g)	$\delta^{15}N$ (‰)
U1545A-																
4H1	146–151	25.0	2529	+8.4	110.71	+13.9	145.1	+7.3	113.1	+6.5	258.2	+7.0	2160	+8.3	89.85	+10.4
8H1	146–151	63.0	2543	+12.2	553.50	+13.1	142.5	+8.0	162.9	+7.0	305.4	+7.5	1684	+12.7	378.6	+11.6
17F2	141–146	141.4	2243	+11.0	423.83	+13.4	160.5	+8.5	109.1	+9.8	269.6	+9.0	1550	+10.7	368.2	+9.5
47F2	107–112	274.7	2103	+16.5	689.87	+13.9	219.6	+11.1	130.9	+9.6	350.5	+10.5	1062	+20.1	565.0	+10.3
55X3	129–144	326.7	2423	+13.4	582.87	+13.5	343.6	+10.6	138.3	+9.5	482.0	+10.3	1358	+14.5	282.7	+9.8
62X1	135–150	392.9	2696	+9.9	450.64	+13.4	759.2	+9.4	747.8	+9.4	1507.0	+9.4	738	+8.9	86.26	+10.2
	Average			+11.9		+13.5		+9.2		+8.6		+8.9		+12.5		+10.3
	S.D.			2.6		0.3		1.3		1.4		1.3		4.0		0.6

* Concentrations of each N in 1 g dry sediment.
** Organic -N contents and $\delta^{15}N$ values were calculated from the other three data of solid phase nitrogen (see text).
*** Calculate the amount of IW fluid contained in 1 g dry sediment using the dry- and wet-density data from the online database, LIMS Reports of IODP (https://web.iodp.tamu.edu/LORE/).

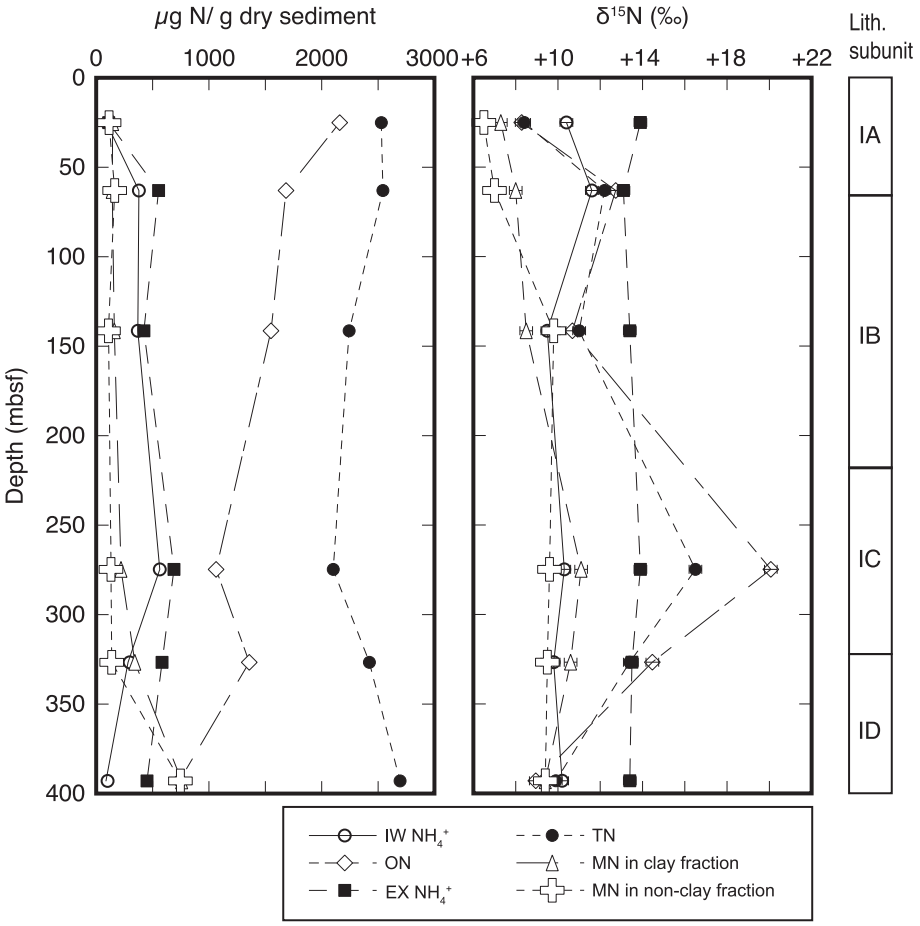

Fig. 4. Downhole profiles for the nitrogen contents (μg N/g dry sediment) and their $\delta^{15}N$ values of TN, ON, IW, MN, and EX ammonium in the six selected samples from Hole U1545A. Contents and $\delta^{15}N$ values of ON were calculated from the nitrogen contents and mass balance of TN, MN, and EX ammonium. See the text for details.

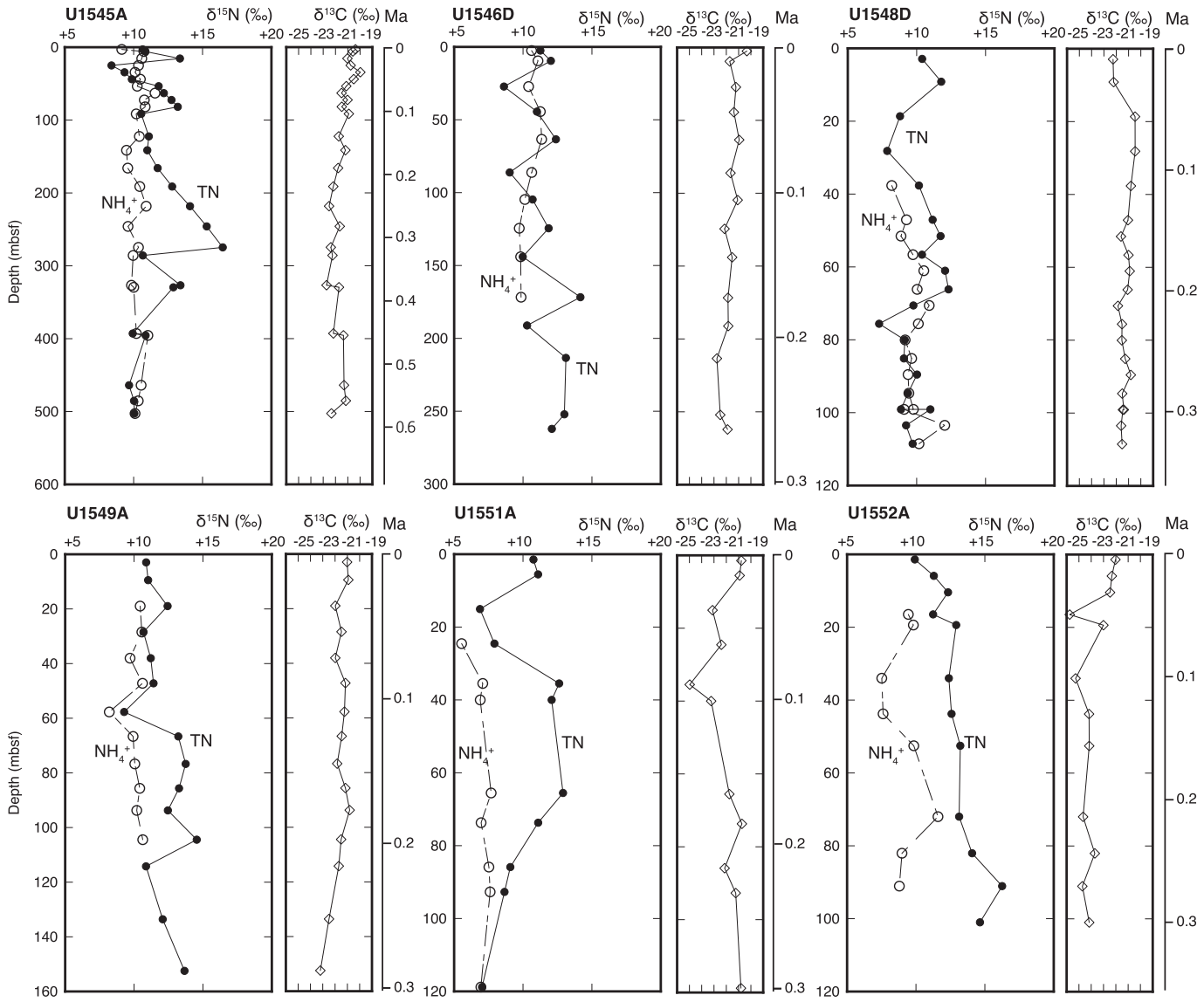

Fig. 5. Downhole profiles for the $\delta^{15}N$ values of TN (filled circle) and IW ammonium (open circle) and $\delta^{13}C$ values of TOC (open diamond) from the six holes studied. Right Ma scales are tentative age models based on microfossil records observed onboard (Teske et al., 2021a). Each analytical error was smaller than the size of each symbol.

Table 4
Clay mineral compositions and the modified Lanson index of the clay fractions (< 2 μm) in the selected six sediment samples from Hole U1545A obtained by XRD analysis.

		wt%	wt% in clay fraction (total 100%)					
Core, Section	Depth (mbsf)	clay content*	smectite	I-S	illite	chlorite	kaolinite	MLI**
U1545A-								
4H1	25.0	38.2	32	5	43	11	9	0.009
8H1	63.0	35.6	36	5	40	12	8	0.022
17F2	141.4	40.7	36	4	43	7	9	0.025
47F2	274.7	38.6	55	8	31	3	3	0.031
55X3	326.7	48.2	61	4	30	1	4	0.021
62X1	392.9	49.6	61	7	26	1	5	0.020

* Clay contents in the bulk sediment (squeezed cake).
** MLI (Modified Lanson Index) are calculated followed by Kuwahara et al. (2001).

region (Petit et al., 2006; Stuart, 2004). Also, the wavenumber of N-H stretching was detected within 2800–3200 cm^{-1} (Petit et al., 1999; Petit et al., 2006; Stuart, 2004). The clay fraction samples contain only small amounts of MN in the interlayers, as mentioned above. However, there were trace levels of absorption with a wide range of weak vibrations within the ammonium-region, suggesting that the MN in the clay fraction is possibly ammonium-fixed in the interlayers of the clay minerals. The other major absorption, such as around 3600–3650 cm^{-1}, is considered to be attributed to O-H stretching, which is associated with the hydroxyl group in clay minerals. The O-H stretching region for clay minerals has been reported to have a wide range (from 3800 to 3400 cm^{-1}), and there is a number of bands observed (Stuart, 2004). Differences in the wavenumber of O-H stretching are often seen in clay minerals containing Mg (II) or Fe (II) in an octahedral sheet (Stuart, 2004; Vaculíková and Pelevová, 2005; Wang et al., 2017) and are also affected by crystallinity (Decarreau et al., 2008; Vedder, 1964).

4. Discussion

4.1. Cause of the fluctuation for $\delta^{15}N_{TN}$ and $\delta^{13}C_{TOC}$ values

Among the proxies of nitrogen measured in this study, only $\delta^{15}N_{TN}$ varies significantly. The variability of this parameter is interpreted to reflect almost entirely the variability of ON. Hence, $\delta^{15}N_{TN}$ fluctuations are inferred to be caused by changes in $\delta^{15}N$ from primary producers, i.e., phytoplankton such as marine diatoms.

In the central Gulf of California, abrupt shifts in $\delta^{15}N_{OM}$ value coincide with global climatic changes during deglaciation and gradual Holocene changes (Pride et al., 1999). According to the reported data by Pride et al. (1999), characteristically high $\delta^{15}N$ values (> +14 ‰) with higher opal accumulation rates were observed in the laminated sediments deposited in the two deglacial stages, the Bølling-Allerød and Preboreal intervals after the Last Glacial Maximum. These abrupt changes have been attributed to the expansion and persistence of suboxic subsurface waters from the entrance of the gulf to Guaymas Basin or further north, which enhance denitrification and lead to enrichment in ^{15}N of nitrate assimilated by primary producers in the gulf (Altabet et al., 1999). The extent is caused by variations in upwelling, vertical mixing, and/or the latitudinal position of the intertropical convergence zone (Pride et al., 1999). Although the published data could only go back to 17 ka, a similar situation may have continued to operate in the central gulf during the Holocene.

A rough estimation of the sedimentation rates for each hole have been proposed based on micropaleontological records (Teske et al., 2021a). Accordingly, in the case of Hole U1545A, which refers to a sedimentation rate of 863 m/Myr, the peak of $\delta^{15}N_{TN}$ value at 15 mbsf may correspond to the Bølling-Allerød warm period (c. 14 ka) and the other peaks at 80 and 275 mbsf may correspond to marine isotope stage (MIS) 5 and 9 (c. 0.12 and 0.31 Ma), respectively. Concerning the other holes, the depths of *c.* 60 and *c.* 40 mbsf in the Holes U1548D (>524 m/Myr) and U1551A (>410 m/Myr), respectively, possibly correspond to Bølling-Allerød warm period. Thus, these significant fluctuations of $\delta^{15}N_{TN}$ values are most likely to reflect the variation of the $\delta^{15}N$ values of primary produces, which coincide with glacial–interglacial climatic changes. Detailed age models for this IODP expedition will be published elsewhere.

In addition to changes that are common throughout all the holes, the differences in C/N and $\delta^{13}C_{TOC}$ values among the holes possibly reflect a variation of source organic matters because those values have been used as proxies for source organic matter (Emerson and Hedges, 1988; Meyers, 1994). Low C/N values (e.g., <10), along with high $\delta^{13}C_{TOC}$ (around −22 ‰) suggest predominance of primary input, i.e., phytoplankton which has the Redfield ratio (C/N value = 106/16 = 6.63). The average $\delta^{13}C_{TOC}$ values of each hole studied are −22.0 to −21.3 ‰ with one exception in Hole U1552A whose average $\delta^{13}C_{TOC}$ value is −23.9 ‰. The organic matter concentration in samples from Hole U1552A, which are depleted in ^{13}C, is higher (average 3.42 wt%) than that in the other holes (1.89–2.49 wt%). The average C/N value (~6.4) is lower in Hole U1552A than in the other holes (8.8–12.7) and terrigenous plants (C/N value >20; Emerson and Hedges, 1988; Meyers, 1994). Site U1552 also is a location of active hydrocarbon gas (mainly methane) advection (Teske et al., 2021a), therefore chemosynthetic microbial activities, especially thioautotrophs, may affect the $\delta^{13}C_{TOC}$ signature, since the carbon isotopic ratios of thioautotrophic microbes that use the Calvin cycle involving RuBisCO (ribulose 1,5-bisphosphate carboxylase/oxygenase) for carbon fixation have a relatively narrow range of $\delta^{13}C$ values, namely −35 ± 5 ‰ (e.g., Nelson and Fisher, 1995). The low C/N value detected in this hole also supports this idea because microbe biome has a low C/N value of 4.2–4.7 (Fagerbakke et al., 1996). If the $\delta^{13}C$ and C/N values can be explained by a two end-member mixing

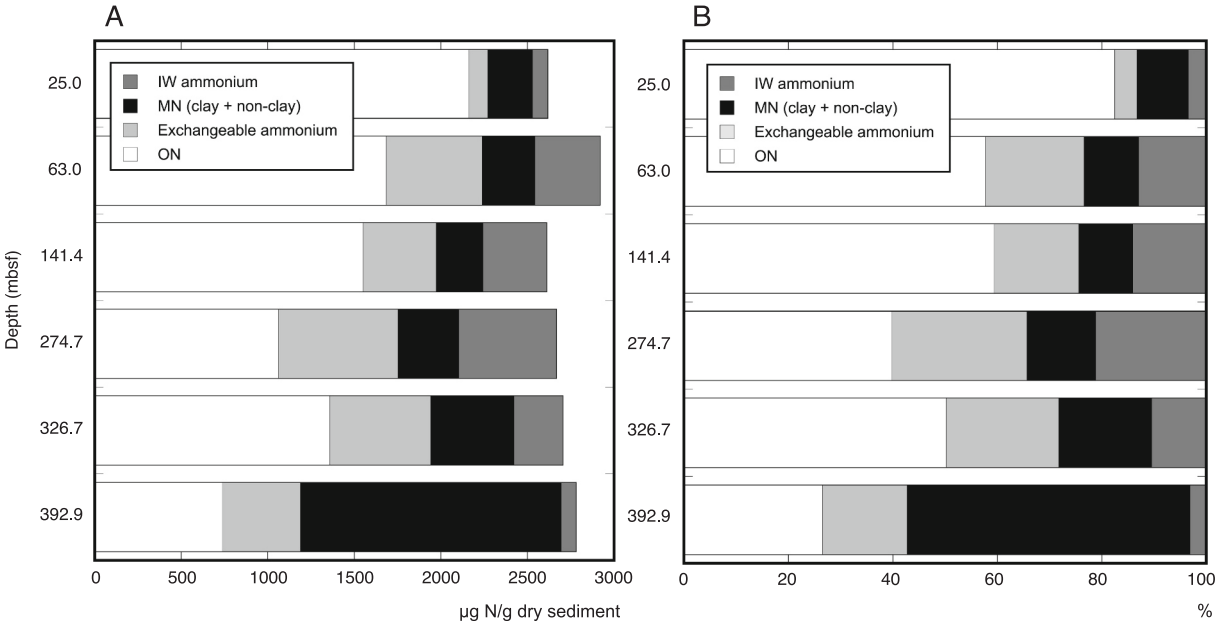

Fig. 6. Stacked (A) and percentage (B) bar charts for the contents of ON, IW, MN and EX ammonium in the six selected samples from Hole U1545A.

model (one end-member is phytoplankton: −22 ‰ and 6.6, respectively), the contributions of thioautotrophic production can be reasonably estimated as *c*. 10–30% and *c*. 10–24%, respectively. On the other hand, the average C/N value of Hole U1551A is the highest (12.7) among all holes drilled. This may be due to the relatively high input of sandy clastic particles which contain terrigenous organic matter documented for this site by Teske et al. (Teske et al., 2018; Teske et al., 2021a).

4.2. Distribution of nitrogen in deep sediments of Hole U1545A

The total content of nitrogen (sum of TN and IW ammonium contained in 1-g dry sediment) in the sediments of Hole U1545A range from 2612 to 2921 μg N/g dry sediment (Table 3 and Fig. 6A) and did not show a significant difference among the samples. On the other hand, the contents of ON (calculated from the other solid phase nitrogen contents), MN and IW ammonium exhibit noticeable changes (Fig. 6). The contents of MN in the clay and non-clay fractions are relatively low to the depth of 274.7 mbsf, but the deepest sample (392.9 mbsf) contains a significant amount of MN (54% and 1.5 mg N/g dry sediment). This depth corresponds to the lithostratigraphic subunit ID, that is recognized by the start of illitization. Thus, the rapid increase of MN contents reflects an increase of fixed ammonium in the interlayer space of clay minerals. Although the calculated crystallinity of illite (MLI) in Table 4 is very low (< 0.1) throughout the hole, fixation of ammonium into illite and other minerals is expected to enhance with advancing diagenesis. The lithostratigraphic subunit ID likely corresponds to the middle diagenetic stage.

Although the proportion of EX ammonium in the shallowest sample of Hole U1545A (25 mbsf) is relatively low (< 5%), at other depths, it accounts for 16–26% of the solid-phase of nitrogen, reaching a maximum at 274.7 mbsf, the same depth at which the content of IW ammonium also reaches a maximum (Fig. 3; Teske et al., 2021a). All the six samples of Hole U1545A are rich in smectite (Table 4), whereas the IW ammonium content in the shallowest sample is very low. Therefore, the low proportion of EX ammonium in the shallowest sample reflect the low release of ammonium from associated organic matter, while the samples deeper than 50 mbsf can adsorb abundant ammonium in smectite interlayers from IW rich in ammonium. The FT-IR spectra also indicate the existence of EX ammonium as a small signal of N-H stretching at 3400–2800 cm^{-1} wavenumber (Pironon et al., 2003) in all the six samples.

The content of IW ammonium in the deeper layers sharply decreases downhole below 300 mbsf (Table 3 and Figs. 3 and 4). This decrease is generally interpreted as resulting from adsorption of ammonium by clay minerals (Müller, 1977; Itihara, 1992), and a decrease in the concentration of potassium in IW (Fig. 3), suggesting the adsorption of these anions by clay minerals (Teske et al., 2021a). However, the decrease in IW ammonium contained in 1 g of dry sediment may be also due to a decrease in IW itself because of compaction. The IW contents of Hole U1545A cores decreased almost linearly until 300 mbsf, but below this depth the contents dropped sharply (Teske et al., 2021a). The fate of IW in the deep sediments is unknown, but migration of water may be plausible. Vertical migration is not so significant to homogenize the concentrations with depth and do not show a convex profile for each dissolved ion in IW (Teske et al., 2021a), but dissolved ions probably mix with adjacent layers by advective transport of solute at the fast accumulation rate in the basin ($\approx 2 \times 10^{-6}$ m/day; Prokopenko et al., 2006). In addition to the vertical mixing, horizontal migration along the strata is possible. The phase transformation of opal-A into opal-CT occurs between the lithostratigraphic subunits IC and ID. Opal-A contains up to 17% weight of structural water (Hurd and Theyer, 1977) that is released during the stepwise dissolution–reprecipitation process of converting opal-A into metastable opal-CT and finally into stable quartz. Additionally, the released structural water of smectite may lead to the compaction of about 10–15% of the bulk volume (Burst, 1969). The released water can be identified as clear depletion of chloride ions at around 300 mbsf in Hole U1545A (Teske et al., 2019). As a result of the transformation and compaction, silica diagenesis is likely to induce fluid flow by the collapse of pore space (Eichhubl and Behl, 1998). Such a partial increase of permeability in the layer is expected to induce lateral migration of IW. The latter may eventually ascend to the seafloor along faults, fissures, or mafic intrusions.

4.3. Source of MN and nitrogen isotope fractionation of ammonium between solid and fluid phases

The $\delta^{15}N_{MN}$ values are lower (~4‰) than those of the other species of nitrogen in sections close to the surface (~100 mbsf) or almost the same (+9 − +11‰) as those of IW ammonium (*c*. +10‰) in the deeper interval (>100 mbsf) in Hole U1545A (Fig. 4). Such homogenized $\delta^{15}N_{IW\text{-}amm}$ values in the deeper interval may be due to mixing of the IW ammonium by advection through the sediment column (Prokopenko et al., 2006). On the other hand, the lower $\delta^{15}N_{MN}$ values closer to the surface (< 100 mbsf), where the MN contents are lower than those in the deeper interval, may suggest that the minerals containing MN are detrital clays and the source of the nitrogen in the minerals possibly is decomposition product from terrigenous organic matter, since the $\delta^{15}N$ values of terrigenous plants are close to 0 ‰ (Wada and Hattori, 1976). The shallowest sample in Hole U1545A showed a significant amount of illite, which indicates that detrital illite has been continuously supplied to the site. Although occurrence of microbially induced smectite-to-illite reaction has been proposed at diagenetic temperatures of up to 80 °C (Kim et al., 2019), it is expected that detrital illite and other nitrogen-bearing minerals possibly incorporated ^{15}N-depleted ammonium on land and transported it to the drilled site of deposition as mentioned by Müller (1977). At the deeper intervals, ammonium-fixed authigenic minerals such as illite, which are enriched in ^{15}N, are considered to occur in addition to the detrital illite, leading to increased $\delta^{15}N_{MN}$ values. If the $\delta^{15}N_{MN}$ values of each layer can be explained by a two end-member mixing model, one is detrital ($\delta^{15}N = +6.5$ ‰, which is minimum $\delta^{15}N_{MN}$ value in Table 3) and the other is EX ammonium ($\delta^{15}N = +13.5$ ‰, which is the average $\delta^{15}N_{EX\text{-}amm}$ value), contribution of the detrital minerals is about 80% or less (37–63%) at the deeper intervals.

The $\delta^{15}N_{EX\text{-}amm}$ values are higher than those of the other types of nitrogen in each layer of the cored sedimentary succession in Hole U1545A while those of IW ammonium are about 3.5 ‰ lower except for one sample at 63 mbsf where the difference in $\delta^{15}N$ values is small (1.6 ‰) and IW ammonium content is the second highest in the U1545A cores. The $\delta^{15}N_{EX\text{-}amm}$ value at this depth may be affected by IW ammonium that is relatively depleted in ^{15}N. The equilibrium isotope fractionation factors of nitrogen between mineral and fluid have been calculated using first-principle methods established by Li et al. (2021), suggesting that ammonium in the natural ammonium-bearing clay minerals including tobelite (ammonium mica) are 1.5–2.3 ‰ enriched in ^{15}N relative to fluid phase ammonium at the low-temperature condition (≤100 °C). Another laboratory study showed slightly higher fractionation (~3 ‰) during ammonium adsorption by clay colloids (Karamanos and Rennie, 1978). Although, in this study, the differences in $\delta^{15}N$ value (~3.9 ‰) between mineral (EX ammonium) and IW ammonium in marine sediments are slightly higher than those reported by previous studies except for the one data point at the depth of 63 mbsf in Hole U1545A. On the other hand, the isotope fractionation factor between ammonium-bearing clay and fluid-phase ammonium is expected to depend on the equilibrium temperature (1.66 at 20 °C and 1.23 at 80 °C; Li et al., 2021), but our result suggests that the change in fractionation factor (3.2–3.9 with ±0.3 analytical error and one exception 1.6 ± 0.3 at 63 mbsf) with increasing burial depth (~100 °C) is insignificant. Further examination is required to understand the isotope fractionation of ammonium-bound N between solid and fluid phases during authigenesis of illite and subsequent diagenesis.

4.4. Possible alteration of $\delta^{15}N_{TN}$ values as a proxy for $\delta^{15}N_{ON}$ during early to middle diagenetic stages and behavior of deep burial ammonium

In the deeper interval, corresponding to the lithostratigraphic subunit IC and ID (> 220 mbsf), the ON contents are lower than 50%. In the same interval, the difference in $\delta^{15}N$ values between TN and ON becomes significant (≥ 1 ‰) over the analytical error range (±0.3 ‰). Although we cannot unveil why the $\delta^{15}N_{MN}$ values are close to $\delta^{15}N_{IW\text{-}amm}$ instead of $\delta^{15}N_{EX\text{-}amm}$, the calculated $\delta^{15}N_{ON}$ based on mass balance is constrained by $\delta^{15}N$ values of MN and/or EX ammonium under the minor ON condition. It means, if $\delta^{15}N_{TN}$ is an intermediate value between $\delta^{15}N_{EX\text{-}amm}$ and $\delta^{15}N_{MN}$, the resulting $\delta^{15}N_{ON}$ value is close to $\delta^{15}N_{TN}$, while the higher $\delta^{15}N_{TN}$ value relative to $\delta^{15}N_{EX\text{-}amm}$ is caused by more enriched $\delta^{15}N_{ON}$. Conversely, lower $\delta^{15}N_{TN}$ value relative to $\delta^{15}N_{MN}$ leads to more depleted $\delta^{15}N_{ON}$. Thus, the homogenous $\delta^{15}N_{IW\text{-}amm}$ and $\delta^{15}N_{EX\text{-}amm}$ values with a certain difference (up to 3.9 ‰ in this study) may contribute to reduced fluctuation of the $\delta^{15}N_{TN}$ with depth after proportion of ON decreases significantly with increasing depth. But it should be noted that the primary $\delta^{15}N_{ON}$ value established on the seafloor is also possibly altered according to the increase of burial depth due to proceeding biodegradation and mineralization (e.g., Robinson et al., 2012, Freudenthal et al., 2001). So, this study does not refute that $\delta^{15}N_{TN}$ value as a proxy of primary $\delta^{15}N_{ON}$ value is still valid.

During diagenesis, the proportion of MN in sediments generally increases together with phase transformation of clay mineral smectite to illite via I/S minerals (e.g., Itihara, 1992). As a result, nitrogen in sedimentary rocks deposited during the Eocene and older epochs is dominated by MN (>50% of TN; Itihara, 1992). In this study the MN contents suddenly increase >50% at the deepest layer (392.9 mbsf), where they correspond to lithostratigraphic subunit ID and smectite to illite transformation (Teske et al., 2021a). The formation age of the layer of about 0.45 Ma (Fig. 5) is very young for significant amount of MN to occur relative to the previous study mentioned above, but a high geothermal gradient in the basin (225 °C/km at Site U1545, Teske et al., 2021a) possibly enhances diagenesis, i.e., the subunit ID reaches middle diagenetic stage. At late diagenetic stage, the sediment is ultimately lithified to sedimentary rock, where IW is almost gone. If EX ammonium is fixed in authigenic clay as MN during diagenesis without apparent isotope fractionation as previously suggested, our results indicate that it is not significantly changed. Instead the $\delta^{15}N_{TN}$ value was possibly altered within a few per mil (‰), probably enriched in ^{15}N relative to ON, after IW that contained ^{15}N-depleted ammonium was expelled from the layer as discussed in the previous section.

A part of EX ammonium in the interlayer of smectite is thought to be expelled into pore spaces during illitization together with water. Those components expelled from the solid phase during diagenesis can be expected to fertilize the deep subseafloor environment, sustaining microbes in deep subsurface biosphere. Clay minerals, especially smectite, play an important role in transporting substances to sustain deep subsurface life. In order to support such speculations, the datasets from only six layers are too sparse, so higher-resolution data and the deeper samples will be required.

In this study, we discussed only ammonium derived from organic matter in the associated sediments. However, ammonium can migrate from the deep-subsurface by volcanic and hydrothermal activities (Jo et al., 2018). Therefore, further studies about the interaction between solid and fluid during ammonium fixation contribute to understand the geochemical cycle of nitrogen through the lithosphere.

5. Conclusion

The $\delta^{15}N_{TN}$ values in the six IODP Expedition 385 holes studied show significant variation with depth, with higher $\delta^{15}N_{TN}$ values possibly corresponding to the Bølling-Allerød warm period (c. 14 ka) as well as MIS 5 and 9 (c. 0.12 and 0.31 Ma, respectively) interglacial periods based on the estimated sedimentation rates. On the other hand, as noted by a previous Ocean Drilling Program report (Prokopenko et al., 2006) and some other studies, there is no noticeable isotopic difference between IW ammonium and TN in marine sediments, whereas the variation in $\delta^{15}N_{IW\text{-}amm}$ is small compared with the $\delta^{15}N_{TN}$ values of each hole. This suggests that because of the advective transport of IW ammonium through the sedimentary layers, the $\delta^{15}N_{IW\text{-}amm}$ values smooth with depth. Also, in Hole U1545A cores the variation in $\delta^{15}N_{EX\text{-}amm}$ is small and approximately 3 ‰ higher than $\delta^{15}N_{IW\text{-}amm}$ values, suggesting that $\delta^{15}N$ values of ammonium are considered to reach an isotopic equilibrium between solid and fluid phases at each layer. The proportions of ON decrease with depth and drop below 50% in this deeper interval (>270 mbsf). In this interval, differences between $\delta^{15}N_{ON}$ and $\delta^{15}N_{TN}$ become significant (≥ 1 ‰) and, thus, are expected to reduce the range of fluctuation in $\delta^{15}N_{TN}$ relative to that of $\delta^{15}N_{ON}$ through the interval. With advancing diagenesis further ammonium is fixed in clay minerals, contributing to an increasing proportion of MN as part of TN as observed at the deepest layer (MN > 50%), suggesting that the $\delta^{15}N_{TN}$ in deep marine sediments may be altered within a few ‰ relative to the $\delta^{15}N_{ON}$.

Supplementary data to this article can be found online at https://doi.org/10.1016/j.chemgeo.2024.122203.

CRediT authorship contribution statement

Toshiro Yamanaka: Conceptualization, Methodology, Writing – original draft. **Arisa Sakamoto:** Investigation. **Kanon Kiyokawa:** Investigation. **Jaeguk Jo:** Investigation, Data curation, Visualization. **Yuji Onishi:** Data curation, Visualization. **Yoshihiro Kuwahara:** Investigation, Data curation, Visualization. **Ji-Hoon Kim:** Investigation. **Lucie C. Pastor:** Investigation. **Andreas Teske:** Project administration. **Daniel Lizarralde:** Project administration. **Tobias W. Höfig:** Data curation, Writing – review & editing.

Declaration of competing interest

The authors declare the following financial interests/personal relationships which may be considered as potential competing interests:

Toshiro Yamanaka reports financial support was provided by the Ministry of Education, Culture, Sports, Science and Technology of Japan. If there are other authors, they declare that they have no known competing financial interests or personal relationships that could have appeared to influence the work reported in this paper.

Data availability

Data will be made available on request.

Acknowledgments

We sincerely thank the IODP technical staff and the R/V *JOIDES Resolution* crew of Expedition 385 for their invaluable assistance. Dr. Chitoshi Mizota helped us with recovery of ammonium using the steam distillation technique, XRD analyses, and clay mineral separation and provided many useful comments to an early version of this manuscript. We appreciate the valuable comments given by Dr. Eva Stüeken, Dr. Benjamin Uveges, Dr. Vasileios Mavromatis and two other anonymous reviewers. T.Y. acknowledges support from the Ministry of Education, Culture, Sports, Science and Technology (MEXT) of Japan through a Grant-in-Aid for Scientific Research (C) (18K03756) and Scientific Research (B) (21H01590 and 21H01172).

References

Altabet, M., Pilskaln, C., Thunell, R., Pride, C., Sigman, D., Chavez, F., Francois, R., 1999. The nitrogen isotopic biogeochemistory of sinking particles from the margin of the Eastern North Pacific. Deep Sea Res. Part I 46, 655–679. https://doi.org/10.1016/S0967-0637(98)00084-3.

Black, C.A., Evans, D.D., Ensminger, L.E., Clark, F.E., White, J.L., Dinauer, R.C., 1965. Methods of Soil Analysis. Part 2. Chemical and Microbiological Properties. American Society of Agronomy, Inc., Publisher Madison, Wisconsin, U.S.A.

Bräuer, K., Hahne, K., 2005. Methodological aspects of the ^{15}N-analysis of Precambrian and Palaeozoic sediments rich in organic matter. Chem. Geol. 218, 361–368. https://doi.org/10.1016/j.chemgeo.2005.01.004.

Bremner, J.M., Edwards, A.D., 1965. Determination and isotope-ratio analysis of different forms of nitrogen in soil. 1. Apparatus and procedure for distillation of ammonium. Soil Sci. Soc. Am. Proceedings 29, 504–507.

Burst, J.F., 1969. Diagenesis of Gulf Coast clayey sediment sand its possible relation to petroleum migration. Am. Assoc. Pet. Geol. Bull. 53, 73–93.

Decarreau, A., Petit, S., Martin, F., Farges, F., Vieillard, P., Joussein, E., 2008. Hydrothermal synthesis, between 75 and 150°C, of high-charge, ferric nontronites. Clay Clay Miner. 56, 322–337. https://doi.org/10.1346/CCMN.2008.0560303.

Eichhubl, P., Behl, R.J., 1998. Diagenesis, deformation, and fluid flow in the Miocene Monterey Formation of coastal California. In: Eichhubl, P. (Ed.), Diagenesis, Deformation, and Fluid Flow in the Miocene Monterey Formation, 83. Pacific Section SEPM Special Publication, pp. 5–13.

Emerson, S., Hedges, J.I., 1988. Processes controlling the organic carbon content of open ocean sediments. Paleoceanogr. Paleoclimatol. 3, 621–634. https://doi.org/10.1029/PA003i005p00621.

Fagerbakke, K.M., Heldal, M., Norland, S., 1996. Content of carbon, nitrogen, oxygen, sulfur and phosphorus in native aquatic and cultured bacteria. Aquat. Microb. Ecol. 10, 15–27. https://doi.org/10.3354/ame010015.

Freudenthal, T., Wagner, T., Wenzhöfer, F., Zabel, M., Wefer, G., 2001. Early diagenesis of organic matter from sediments of the eastern subtropical Atlantic: evidence from stable nitrogen and carbon isotopes. Geochim. Cosmochim. Acta 65, 1795–1808. https://doi.org/10.1016/S0016-7037(01)00554-3.

Gieskes, J.M., Gamo, T., Brumsack, H., 1991. Chemical methods for interstitial water analysis aboard JOIDES Resolution, 15. Ocean Drilling Program Texas A&M University. Technical Note, pp. 40–45.

Holloway, J.M., Dahlgren, R.A., 2002. (2002) Nitrogen in rock: occurrences and biogeochemical implications. Glob. Biogeochem. Cycles 16, 1118. https://doi.org/10.1029/2002gb001862.

Honma, H., Itihara, Y., 1981. Distribution of ammonium in minerals of metamorphic and granitic rocks. Geochim. et Cosmochim. Acta. 45 (6), 983–988. https://doi.org/10.1016/0016-7037(81)90122-8.

Hurd, D.C., Theyer, F., 1977. Changes in the physical and chemical properties of biogenic silica from the central equatorial Pacific: Part II. Refractivity index, density, and water content of acid-cleaned samples. Am. J. Sci. 277, 168–1202.

Itihara, Y., 1992. Recent studies on ammonium in rocks. J. Geol. Soc. Jpn. 98, 885–899 (in Japanese with English abstract).

Jo, J., Yamanaka, T., Kashimura, T., Okunishi, Y., Kuwahara, Y., Kadota, I., Miyoshi, Y., Ishibashi, J.-I., Chiba, H., 2018. Mineral nitrogen isotope signature in clay minerals formed under high ammonium environment conditions in sediment associated with ammonium-rich sediment-hosted hydrothermal system. Geochem. J. 52, 317–333. https://doi.org/10.2343/geochemj.2.0518.

Karamanos, R.E., Rennie, D.A., 1978. Nitrogen isotope fractionation during ammonium exchange reactions with soil clay. Can. J. Soil Sci. 58, 53–60. https://doi.org/10.4141/cjss78-005.

Kim, J., Dong, H., Yang, K., Park, H., Elliott, W.C., Spivack, A., Koo, T.-h., Kim, G., Morono, Y., Henkel, S., Inagaki, F., Zeng, Q., Hoshino, T., Heuer, V.B., 2019. Naturally occurring, microbially induced smectite-to-illite reaction. Geology 47, 535–539. https://doi.org/10.1130/G46122.1.

Kuwahara, Y., Fuji, R., Sakai, H., Masudome, Y., 2001. Measurement of crystallinity and relative amount of clay minerals in the Kathmandu Basin sediments by decomposition of XRD patterns (profile fitting). J. Nepal Geol. Soc. 52 (Sp. Issue), 71–80. https://doi.org/10.3126/jngs.v25i0.32056.

Lanson, B., 1997. Decomposition of experimental X-ray diffraction patterns (profile fitting): a convenient way to study clay minerals. Clay Clay Miner. 45, 132–146.

Li, Y., Li, L., Wu, Z., 2021. First-principles calculations of equilibrium nitrogen isotope fractionations among aqueous ammonium, silicate minerals and salts. Geochim. Cosmochim. Acta 297, 220–232. https://doi.org/10.1016/j.gca.2021.01.019.

Liang, B.C., Mackenzie, A.F., Gregorich, E.G., 1999. Measurement of fixed ammonium and nitrogen isotope ratios using dry combustion. Soil Sci. Soc. Am. J. 63, 1667–1669. https://doi.org/10.2136/sssaj1999.6361667x.

Manheim, F.T., Sayles, 1974. Composition and origin of interstitial waters of marine sediments, based on deep sea drill cores. In: Golderg, E.D. (Ed.), The Sea 5, 527–568.

Meyers, P.A., 1994. Preservation of elemental and isotopic source identification of sedimentary organic matter. Chem. Geol. 114, 289–302. https://doi.org/10.1016/0009-2541(94)90059-0.

Mizota, C., Sasaki, M., Yamanaka, T., 2007. Temporal variation in the concentration and nitrogen isotopic ratios of inorganic nitrogen from soils under cormorant and Heron colonies. Japan. J. Ornithol. 56, 115–130. https://doi.org/10.2326/jjo.56.115 (in Japanese).

Mizutani, H., Kabaya, Y., Wada, E., 1985. Ammonia volatilization and high $^{15}N/^{14}N$ ratio in a penguin rookery in Antarctica. Geochem. J. 19, 323–327. https://doi.org/10.2343/geochemj.19.323.

Morford, S.L., Houlton, B.Z., Dahlgren, R.A., 2011. Increased forest ecosystem carbon and nitrogen storage from nitrogen rich bedrock. Nature 477, 78–81. https://doi.org/10.1038/nature10415.

Müller, P.J., 1977. CN ratios in Pacific deep-sea sediments: effect of inorganic ammonium and organic nitrogen compounds sorbed by clays. Geochim. Cosmochim. Acta 41, 765–776. https://doi.org/10.1016/0016-7037(77)90047-3.

Murray, R.W., Miller, D.J., and Kryc, K.A., 2000. Analysis of major and trace elements in rocks, sediments, and interstitial waters by inductively coupled plasma–atomic emission spectrometry (ICP-AES). Ocean Drilling Program Technical Note, 29. doi: 10.2973/odp.tn.29.2000.

Mysen, B., 2019. Nitrogen in the Earth: abundance and transport. Prog. Earth Planet Sci. 6, 38. https://doi.org/10.1186/s40645-019-0286-x.

Nelson, D.C., Fisher, C.R., 1995. Chemoautotrophic and Methanotrophic Endosymbiotic bacteria at deep-sea vents and seeps. In: Karl, D.M. (Ed.), The Microbiology of Deep-Sea Hydrothermal Vent Habitats. CRC, Boca Raton, pp. 125–167.

Nieder, R., Benbi, D.K., Scherer, H.W., 2011. Fixation and defixation of ammonium in soils: a review. Biol. Fertil. Soils 47, 1–14. https://doi.org/10.1007/s00374-010-0506-4.

Petit, S., Righi, D., Madejová, J., Decarreau, A., 1999. Interpretation of the infrared NH_4^+ spectrum of the NH_4^+- clays: application to the evaluation of the layer charge. Clay Miner. 34, 543–549. https://doi.org/10.1180/000985599546433.

Petit, S., Righi, D., Madejová, J., 2006. Infrared spectroscopy of NH_4^+-bearing and saturated clay minerals: a review of the study of layer charge. Appl. Clay Sci. 34, 22–30. https://doi.org/10.1016/j.clay.2006.02.007.

Pironon, J., Pelletier, M., De Donato, P., Mosser-Ruck, R., 2003. Characterization of smectite and illite by FTIR spectroscopy of interlayer NH_4^+ cations. Clay Miner. 31, 201–211. https://doi.org/10.1180/0009855033820089.

Pride, C., Thunell, R., Sigman, D., Keigwin, L., Altabet, M.A., 1999. Nitrogen isotopic variations in the Gulf of California since the last deglaciation: response to global climatic change. Paleoceanography 3, 397–409. https://doi.org/10.1029/1999PA900004.

Prokopenko, M.G., Hammond, D.E., Stott, L., 2006. Lack of isotopic fractionation of $\delta^{15}N$ of organic matter during long-term diagenesis in marine sediments, ODP Leg 202, Sites 1234 and 1235. In: Tiedemann, R., Mix, A.C., Richter, C., Ruddiman, W.F. (Eds.), Proceedings of the Ocean Drilling Program, Scientific Results, 202, pp. 1–22. https://doi.org/10.2973/odp.proc.sr.202.207.2006.

Robinson, R.S., Kienast, M., Luiza Albuquerque, A., Altabet, M., Contreras, S., De Pol Holz, R., Dubois, N., Francois, R., Galbraith, E., Hsu, T.-C., Ivanochko, T., Jaccard, S., Kao, S.-J., Kiefer, T., Kienast, S., Lehmann, M., Martinez, P., McCarthy, M., Möbius, J., Pedersen, T., Quan, T.M., Ryabenko, E., Schmittner, A., Schneider, R., Schneider-Mor, A., Shigemitsu, M., Sinclair, D., Somes, C., Studer, A., Thunell, R., Yang, J.-Y., 2012. A review of nitrogen iso- topic alteration in marine sediments. Paleoceanography 27, 1–13. https://doi.org/10.1029/2012PA002321.

Sano, Y., Takahata, N., Nishio, Y., Marty, B., 1998. Nitrogen recycling in subduction zones. Geophys. Res. Lett. 25, 2289–2292. https://doi.org/10.1029/98GL01687.

Schidlowski, M., Hayes, J.M., Kaplan, I.R., 1983. Isotopic inferences of ancient biochemistries: carbon, sulfur, hydrogen and nitrogen. In: Schopf, J.W. (Ed.), Earth's Earliest Biosphere. Princeton Univ. Press, Princeton, NJ, pp. 149–186.

Silva, J.A., 1964. Determination of Fixed Ammonium in Soils. Retrospective Theses and Dissertations. Iowa State University, U.S.A.

Silva, J.A., Bremner, J.M., 1966. Determination and iso- tope-ratio analysis of different forms of nitrogen in soils: 5. Fixed ammonium. Soil Sci. 30, 587–594. https://doi.org/10.2136/sssaj1966.03615995003000050017x.

Steffens, D., Sparks, D.L., 1999. Effect of residence time on the kinetics of nonexchangeable ammonium release from illite and vermiculite. J. Plant Nutr. Soil Sci. 162, 599–604. https://doi.org/10.1002/(SICI)1522-2624(199912)162:6<599::AID-JPLN599>3.0.CO;2-Y.

Stuart, B., 2004. Infrared Spectroscopy: Fundamentals and Applications. John Wiley & Sons, Ltd.

Teske, A., Lizarralde, D., Höfig, T.W., 2018. Expedition 385 Scientific Prospectus: Guaymas Basin Tectonics and Biosphere, International Ocean Discovery Program, College Station, TX (International Ocean Discovery Program). https://doi.org/10.14379/iodp-sp-385-2018.

Teske, A., McKay, L.J., Ravelo, A.C., Aiello, I., Mortera, C., Núñez-Useche, F., Canet, C., Chanton, J.P., Brunner, B., Hensen, C., Ramírez, G.A., 2019. Characteristics and Evolution of sill-driven off-axis hydrothermalism in Guaymas Basin–the Ringvent site. Sci. Rep. 9 (1), 1–16. https://doi.org/10.1038/s41598-019-50200-5.

Teske, A., Lizarralde, D., Höfig, T.W., the Expedition 385 Scientists, 2021a. Guaymas Basin Tectonics and Biosphere. Proceedings of the International Ocean Discovery Program, 385: College Station, TX (International Ocean Discovery Program). https://doi.org/10.14379/iodp.proc.385.2021.

Teske, A., Lizarralde, D., Höfig, T.W., Aiello, I., Ash, J., Bojanova, D., Buatier, M., Edgcomb, V.P., Galerne, C., Gontharet, S., Heuer, V.B., Jiang, S., Kars, M.A.C., Kim, J.H., Koornneef, L.M.T., Marsaglia, K., Meyer, N.R., Morono, Y., Negrete-Aranda, R., Neumann, F., Pastor, L.C., Peña-Salinas, M.E., Perez-Cruz, L., Ran, L., Riboulleau, A., Sarao, J., Schubert, F., Singh, S.K., Stock, J., Toffin, L., Xie, W., Yamanaka, T., Zhuang, G., 2021b. Expedition 385 methods. In: Teske, A., Lizarralde, D., Höfig, T.W., the Expedition 385 Scientists (Eds.), Guaymas Basin Tectonics and Biosphere. Proceedings of the International Ocean Discovery Program. College Station, TX (International Ocean Discovery Program). https://doi.org/10.14379/iodp.proc.385.102.2021.

Vaculíková, L., Pelevová, E., 2005. Identification of clay minerals and micas in sedimentary rocks. Acta Geodyn. Geomater. 2, 167–175.

Vedder, W., 1964. Correlations between infrared spectrum and chemical composition of mica. Am. Mineral. 49, 736–768.

Wada, E., Hattori, A., 1976. Natural abundance of ^{15}N in particulate organic matter in the North Pacific Ocean. Geochim. Cosmochim. Acta 40, 249–251. https://doi.org/10.1016/0016-7037(76)90183-6.

Wang, W., Tian, G., Zong, L., Zhou, Y., Kang, Y., Wang, Q., Wang, A., 2017. From illite/smectite clay to mesoporous silicate adsorbent for efficient removal of chlortetracycline from water. J. Environ. Sci. 51, 31–43. https://doi.org/10.1016/j.jes.2016.09.008.